

## Computer simulation of liquid crystals

*Prabal K Maiti, V. Arun Kumar AND K. G. Ayappa*

**Abstract** | In this article we review the current status in the modelling of both thermotropic and lyotropic Liquid crystal. We discuss various coarse-graining schemes as well as simulation techniques such as Monte Carlo (MC) and Molecular dynamics (MD) simulations. In the area of MC simulations we discuss in detail the algorithm for simulating hard objects such as spherocylinders of various aspect ratios where excluded volume interaction enters in the simulation through overlap test. We use this technique to study the phase diagram, of a special class of thermotropic liquid crystals namely banana liquid crystals. Next we discuss a coarse-grain model of surfactant molecules and study the self-assembly of the surfactant oligomers using MD simulations. Finally we discuss an atomistically informed coarse-grained description of the lipid molecules used to study the gel to liquid crystalline phase transition in the lipid bilayer system.

### Introduction

The liquid crystalline phase is ubiquitous in nature. Based on their phase behaviour, liquid crystals can be classified into either thermotropic or lyotropic liquid crystals. In the case of thermotropic liquid crystals, phase transformations occur as a function of temperature, while in the case of lyotropic liquid crystals, phase change occurs as a function of concentration [1]. Thermotropic liquid crystals are traditionally single component systems which show a wide range of phases, classified based on the positional and orientational order of the molecules, as a function of temperature [2, 3]. These intermediate phases include smectics, nematics and discotics and the formation of a particular phase is related to the chemical structure and architecture of the constituent molecules. Additionally, pressure can also induce phase transformations and replaces the role of temperature. When more than one component is present, then the presence of a given phase is dependent on the concentration of the mixture giving rise to lyotropic liquid crystals. Commonly occurring examples of lyotropic liquid crystals are water-amphiphilic systems where the amphiphilic molecule is characterized by a

hydrophilic head group and a hydrophobic tail. Depending on the balance between the hydrophilic and hydrophobic character of the molecule and the concentration relative to the aqueous phase, lyotropic liquid crystals can arrange into hexagonal, micellar, reverse micellar and lamellar phases [4, 5]. Examples of amphiphilic molecules are surfactants the common ingredients of soaps, and phospholipids which are integral constituents of the cell membrane. Due to the wide range of microstructures possible with liquid crystals these systems are commonly referred to as complex fluids.

In either case, the liquid crystal phase is very sensitive to shape of the molecule. Relating the macroscopic properties of the liquid crystal phase to the microscopic structure of the constituent molecule is a very complex problem. However it is essential to understand the structure-property relationship both from a fundamental point of view as well as for developing potential technologies based on liquid crystals. Due to the large number of interactions and complex geometries involved, it is difficult to develop a predictive theoretical framework for liquid crystals. As a result, computer simulations have emerged as a powerful tool to

*Centre for Condensed  
Matter Theory,  
Department of Physics,  
Indian Institute of  
Science, Bangalore  
Department of Chemical  
Engineering, Indian  
Institute of Science,  
Bangalore  
maiti@physics.iisc.ernet.in*

Figure 1: Models for thin rods: (a) connected spheres and (b) hard spherocylinder with aspect ratio  $L/D$ .

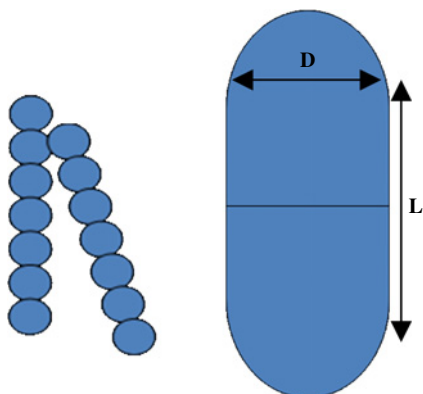
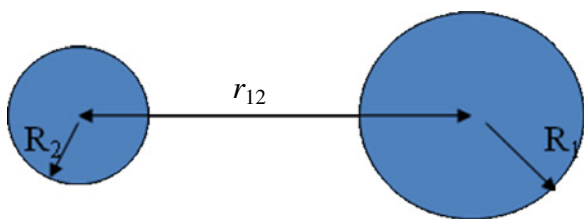


Figure 2: Overlap test for two rigid sphere of radius  $R_1$  and  $R_2$ .



investigate the dependence of the liquid crystal phase behavior to the structure of its constituent molecules [6, 7]. Various levels of description have been used to develop models for liquid crystals. These models include simple spherocylinders or hard-sphere chains which interact through hard or soft excluded-volume repulsion [8–10], molecules with ellipsoidal shape interacting through the Gay-Berne potential [11, 12], and simple “bead-spring” representation of molecules interacting through Lennard-Jones potentials [13]. There are also simulations involving atomic level models of real liquid crystal molecules [14, 15].

Simulation methods employed range from molecular dynamics (MD), Monte Carlo (MC), Brownian dynamics to dissipative particle dynamics. In this review article we give an overview of the various methods used in simulating self-assembly phenomena in liquid crystals. From a microscopic point of view, molecular dynamics is a realistic approach as it considers all atom dynamics, but suffers from the computational effort required to explore the full phase space as well as the longer length and time scales which are present at the mesoscopic level. An effective coarse-grained model

can reduce the computational effort, but lacks the required chemical details to be useful as a predictive tool. The different length and time scales present in complex fluids are the bond length and bond vibration times at the molecular level to the size of colloids, polymer chain lengths and longer relaxation times at the mesoscopic level. The fastest motions are bond and angle vibrational motions, small fluctuations of dihedral angles around a bond within the molecule. These types of motions typically occur on a time scale up to a few picoseconds. The slowest motions in surfactant solutions occur in the range of nanoseconds and are related to the relaxation time of micelles or the lateral diffusion of amphiphilic molecules in the lamellar or bilayer phase. To study these systems which inherently possess widely different length and time scales, multi-scale methods are necessary. Developing suitable multiscale strategies that cover the range of length and time scales typically involved in these complex mesophases is an active area of research [16–18].

In the first part of this review article, we focus on thermotropic liquid crystals where models based on excluded volume interactions can be used to study the wide variety of phases that occur in bent-core or banana shaped liquid crystal molecules using Monte Carlo simulations. In the second part of the review we focus on lyotropic liquid crystals. We discuss coarse-grained models for surfactant self-assembly which are used to study the process of micelle formation in water-gemini surfactant systems using molecular dynamics simulations. Finally we illustrate a coarse grained description that has been constructed to study the thermal behaviour of the lamellar or bilayer phase in a water – phospholipid system. We point out that the complex microstructure depicted by liquid crystal systems have been extensively investigated using computer simulations [19, 20]. In this review we focus on three illustrative systems which we have studied in our laboratory.

### Thermotropic liquid crystal

Hard-core models are particularly appealing due to their simplicity and relative ease of computation, both in simulation and theory. In particular, hard spherocylinders have been widely studied as simple models for conventional liquid crystals [8, 9]. This model exhibits rich phase behaviour which includes the formation of the isotropic, nematic, smectic, columnar, and solid phases. The phase transitions are driven by the competition between two main entropic contributions, the orientational entropy favouring the isotropic phase and the positional entropy favouring the ordered phases, as shown in

the 1940s by Onsager in the limit of infinitely thin rods [21]. Below we give a brief outline of the MC methodology for simulating hard elongated objects like thin rods.

Two types of models of thin rods can be envisaged: it can be viewed as made up of connected spheres as shown in Figure 1a or a spherocylinder as shown in Figure 1b.

Each MC step consists of translation and rotation of the rods. The rotation can be performed using quaternions defined through the Euler angles. A move is accepted if there is no overlap between two rods. Hence an efficient overlap test is the key ingredient in this technique. In the case of rods consisting of spherical objects the overlap test is very simple. Two hard spheres of radius  $R_1$  and  $R_2$  (figure 2) overlap if the distance between the center of the two spheres  $r_{12}$  is less than  $\sigma_{12} = R_1 + R_2$ .

In simulation we do not compare  $r_{12}$  with  $\sigma_{12}$  but  $r_{12}^2$  with  $\sigma_{12}^2$  as the later test is computationally cheaper. However the computational expense is enormous as it involves order of  $N^2$  operation at each MC step where  $N$  is the number of spherical beads in the system. This is overcome if each molecule is considered to be a spherocylinder. The overlap test for spherocylinders is very efficient. Below we outline the key steps. More details can be found out in the brilliant article by Allen and co-workers [22]. The spherocylinder can be thought of as a set of points that are within a distance  $R$  from a line segment of length  $L$ . We can draw around every point on this line segment a sphere of radius  $R$  that contains all points that are within a distance  $R$  from that point.

We would like to determine the minimum distance between two finite line segments  $i$  and

$j$  with orientations  $\hat{u}_i$  and  $\hat{u}_j$  and centers  $r_i$  and  $r_j$ . We can describe any point on line  $i$  parametrically as

$$r_i(\lambda) = r_i + \lambda \hat{u}_i. \quad (1)$$

Line  $j$  is given by

$$r_j(\mu) = r_j + \mu \hat{u}_j \quad (2)$$

The vector distance between these two points is given by

$$r_{ij}(\lambda, \mu) = (r_i - r_j) + \lambda \hat{u}_i - \mu \hat{u}_j \quad (3)$$

Now we want to determine the values of  $\lambda$  and  $\mu$  for which the distance  $r_{ij}$  is minimum. A simple method to find these values of  $\lambda$  and  $\mu$  is the following. Construct the dot product of  $r_{ij}$  (equation 3) with  $\hat{u}_i$  and  $\hat{u}_j$ . The shortest distance vector must be perpendicular to both  $\hat{u}_i$  and  $\hat{u}_j$ . So we need to solve the following equations

$$(r_i - r_j) \cdot \hat{u}_i = -\lambda \hat{u}_i \cdot \hat{u}_j + \mu \hat{u}_j \cdot \hat{u}_i \quad (4)$$

$$(r_i - r_j) \cdot \hat{u}_j = -\lambda \hat{u}_i \cdot \hat{u}_j + \mu \hat{u}_j \cdot \hat{u}_i \quad (5)$$

Solving equations 4 and 5 we get the following values for  $\lambda$  and  $\mu$  which minimizes the distance between the two line segments

$$\begin{pmatrix} \lambda_0 \\ \mu_0 \end{pmatrix} = \frac{1}{1 - (\hat{u}_i \cdot \hat{u}_j)^2} \times \begin{pmatrix} -\hat{u}_i \cdot r_{ij} + (\hat{u}_i \cdot \hat{u}_j)(\hat{u}_j \cdot r_{ij}) \\ +\hat{u}_j \cdot r_{ij} - (\hat{u}_i \cdot \hat{u}_j)(\hat{u}_i \cdot r_{ij}) \end{pmatrix} \quad (6)$$

Figure 3: Various relative orientations for computing overlap criteria for spherocylinders: (a) parallel to each other, (b) perpendicular to each other (c) touching each other in parallel orientation.

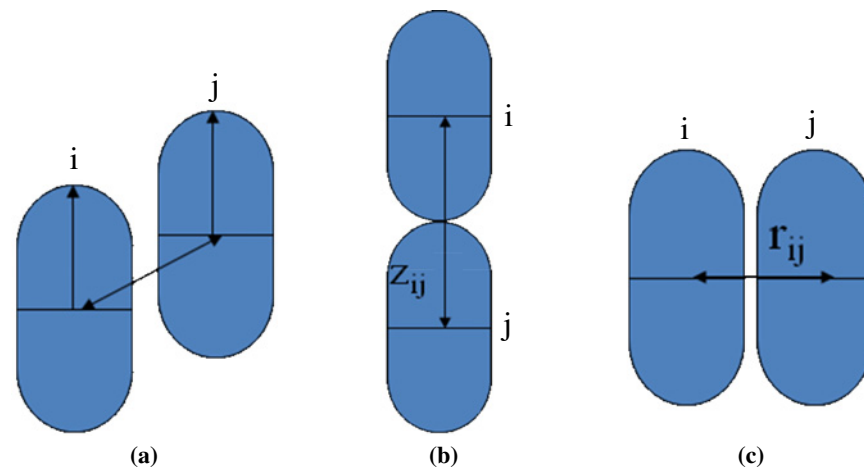
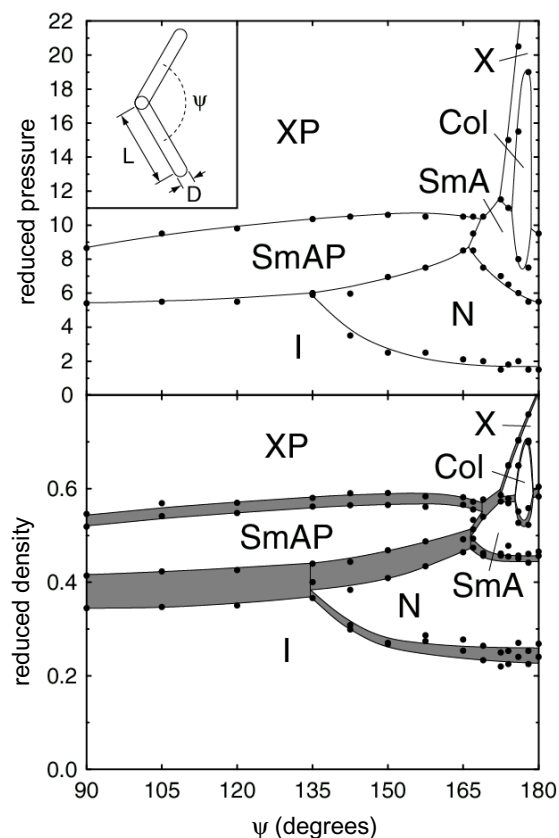


Figure 4: Phase diagram of bent-core liquid crystal as a function of opening angle  $\psi$ , obtained through MC simulation. Various phases are: Isotropic fluid (I), Nematic (N), Polar smectic A (SmAP), Smectic A (SmA), Columnar (Col), Polar crystal (XP), Crystal (X). Reproduced with permission from [25]. Copyright American Physical Society.



Equation 6 is a general expression which helps to check the overlap criteria for any general orientation of the spherocylinders. Below we discuss several special cases for which equation 6 reduces to much simpler form.

**Case I:** If the spherocylinders are parallel to each other as in figure 3 (a) the overlap test reduces to much simpler case as follows. For the parallel case we have

$$r_{ij} \cdot \hat{u}_i = r_{ij} \cdot \hat{u}_j \quad (7)$$

Using the above criteria in equation 6, we get the following values for  $\lambda$  and  $\mu$

$$\begin{aligned} \lambda_0 &= \frac{1}{1 - (\hat{u}_i \cdot \hat{u}_j)^2} (-\hat{u}_i \cdot r_{ij} + (\hat{u}_i \cdot \hat{u}_j)(\hat{u}_j \cdot r_{ij})) \\ &= \frac{-\hat{u}_i \cdot r_{ij}(1 - \hat{u}_i \cdot \hat{u}_j)}{(1 + \hat{u}_i \cdot \hat{u}_j)(1 - \hat{u}_i \cdot \hat{u}_j)} = \frac{-\hat{u}_i \cdot r_{ij}}{2} \end{aligned}$$

Similarly

$$\mu_0 = \frac{\hat{u}_j \cdot r_{ij}}{2} \quad (8)$$

**Case II:** If the spherocylinder are perpendicular to each other the overlap test can be performed by comparing the distance between the centres of the two spherocylinders given by

$$z_{ij} = \frac{L_i}{2} + \frac{L_j}{2} + D \quad (9)$$

If  $z_{ij} < \frac{L_i}{2} + \frac{L_j}{2} + D$  there is overlap between the spherocylinders.

**Case III:** If the spherocylinders are arranged as in figure 3(c), the overlap can be detected if  $r_{ij} < D$ . For all other general orientations of the spherocylinder we have to make series of approximations to find the condition for overlap. In one case we set  $\lambda = |L/2|$  and find out  $\mu$  which will minimize the distance between two spherocylinders. From equation 6 we have

$$\begin{aligned} r_{ij}^2(\lambda, \mu) &= r_{ij}^2 + \lambda^2 + \mu^2 - 2\lambda r_{ij} \cdot \hat{u}_i \\ &\quad + 2\mu r_{ij} \cdot \hat{u}_j - 2\lambda\mu \hat{u}_i \cdot \hat{u}_j \end{aligned} \quad (10)$$

Minimizing the above expression with respect to  $\mu \frac{dr_{ij}^2(\lambda, \mu)}{d\mu} = 0$  we have

$$\mu = \lambda \hat{u}_i \cdot \hat{u}_j - r_{ij} \cdot \hat{u}_j \quad (11)$$

Similarly if we set  $\mu = |L/2|$  and find out  $\lambda$  which will minimize the separation between the spherocylinders we get

$$\lambda = \mu \hat{u}_i \cdot \hat{u}_j - r_{ij} \cdot \hat{u}_i \quad (12)$$

As an example of the application of the MC methods described above we apply this technique to study the various liquid crystal phases of bent core liquid crystal. Bent core LCs are new class of smectic LC phases [23, 24] (SmCP phases) which has attracted tremendous attention in recent past due to its potential application in display and non-linear optical (NLO) devices. These molecules also present a very rare example of spontaneous formation of macroscopic chiral layers from achiral molecules. The molecules comprising these phases have “bow” or “banana” shaped cores (shown in inset of figure 4). We have done MC simulation in a system of 400 banana molecules and mapped out the phase diagram as a function of banana opening angle [25]. Figure 4 gives the detailed phase diagram of the

Figure 5: Final configurations from Monte Carlo simulations of  $N=400$  bent-core molecules with opening angle  $\psi=90^\circ$  as a function of pressure. From left to right: isotropic phase ( $P^*=1$ ), polar smectic A ( $P^*=7$ ), and polar crystal ( $P^*=15$ ).

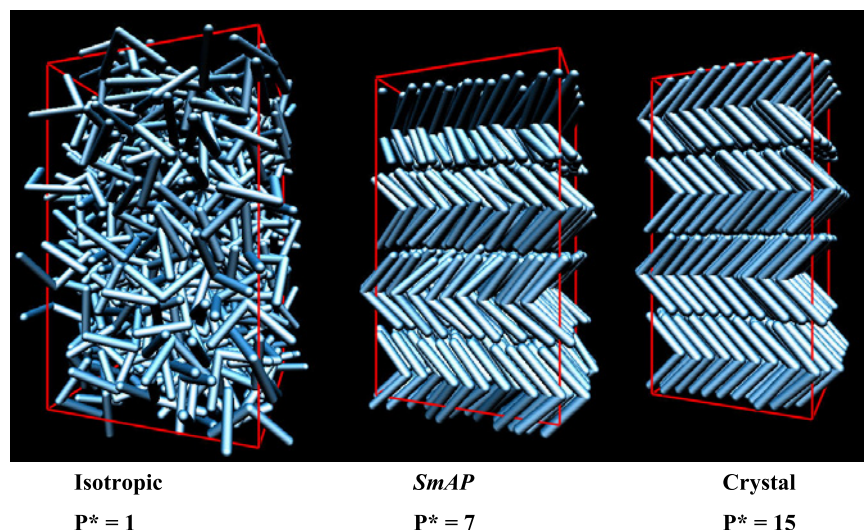
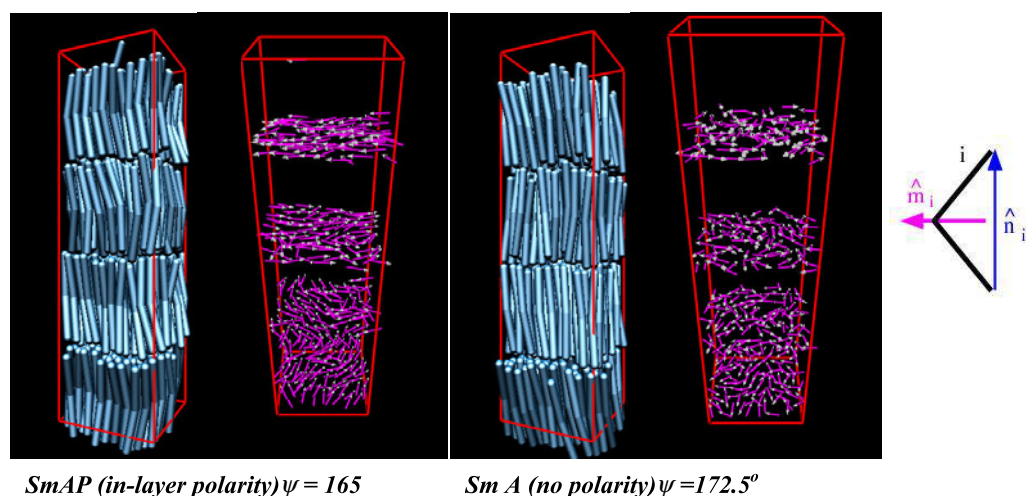


Figure 6: Configuration showing the polar smectic (SmAP) for a opening angle  $\psi=165$  degree. This phase disappears and becomes a non-polar smectic (SmA) at an opening angle of  $\psi=172.5$  degree. We have also shown the in-plane arrangement of the polar vector  $\hat{m}_i$  for both the cases.

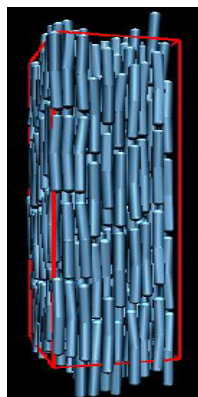


banana molecules. Our MC simulation gives rise to a variety of LC phases such as: Isotropic fluid ( $I$ ), Nematic ( $N$ ), Polar smectic A (SmAP), Smectic A (SmA), Columnar (Col), Polar crystal (XP), Crystal (X). In figures 5 and 6 we give equilibrium snapshots for few LC phases for two opening angles. The Polar smectic A (SmAP) phase exists for certain opening angles above which only the non-polar Smectic A (SmA) is observed. We have monitored the in-plane

polarization of the smectic phase to distinguish between the polar and non-polar phase. The in-plane polarization is calculated as  $\hat{m} = \sum_i \hat{m}_i / N$  where  $\hat{m}_i$  is defined as the bow vector of the banana molecules as shown in figure 6. We also show the equilibrium configuration of the polar and non-polar smectic phases corresponding to the opening angle of 165 and 172.5 degree respectively. Our MC simulation results also demonstrate the existence of



Figure 7: Columnar phase formed at an opening angle of  $\psi = 178$  degree.



the columnar phase for a narrow range of opening angles. Figure 7 shows equilibrium configuration of a columnar phase for an opening angle of 178 degree.

### Self-assembly in Lyotropic liquid crystals

Surfactant molecules are amphiphilic compounds, which display complex phase behavior in the presence of water and/or oil. These amphiphilic molecules are made up of two distinct components, a hydrophilic part which dissolves easily in water (water loving), and a hydrophobic part which is repelled by water (water hating). In aqueous environments, they assemble such that the hydrophobic parts of the molecules are shielded from the water by the hydrophilic ones. In general, hydrophobic groups are long hydrocarbon chains

and hydrophilic groups are polar groups which may be anionic, cationic, non ionic or zwitterionic.

In the presence of water and oil and above the critical micelle concentrations these amphiphilic molecules exhibit different structures like micelles, bilayers and reverse micelles as shown in figure 8, which represents a ternary phase diagram of a water-oil-surfactant system. In the figure, L1 represents a single phase region of oil in water microemulsions. L2 represents a region of reverse micelles i.e., water in oil microemulsions, and D represents the lamellar liquid crystalline phase. These phases emerge due to different concentrations at a fixed temperature. The forces that hold these amphiphilic molecules together in micelles and bilayers arise from weaker van der Waals forces, hydrophobic, hydrogen-bonding and electrostatic interactions. Due to these complex interactions, changing the conditions of the solution, will not only affect the interactions between the aggregates, but will also affect the intermolecular forces in each aggregate, so that the size and the shape of the aggregates will change. Computer simulations are widely used to understand the self-aggregation and phase behaviour in these systems.

Many of these self-assembly phenomena as well as the structure and dynamics of these self-assemble liquid crystalline phases can be studied by means of molecular dynamics or Monte Carlo techniques. We have recently used MD simulations to study the micelle formation in model surfactant oligomer solutions [26]. Surfactant oligomers are new classes of surfactants made of multiple single chain surfactants connected at the head group level by a spacer. One of these classes is the *gemini* surfactants [27–32] consisting of two

Figure 8: Ternary phase diagram of a typical water-oil-surfactant system. The various structures formed at different concentrations are also shown. Blue represent the hydrophilic head groups and red represent the hydrophobic tail groups.

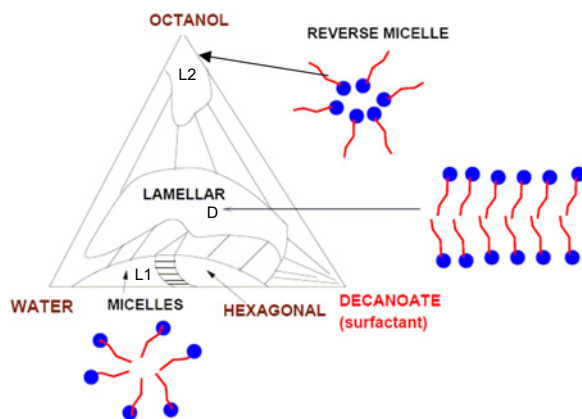


Figure 9: Coarse-grained model of various surfactant oligomers.

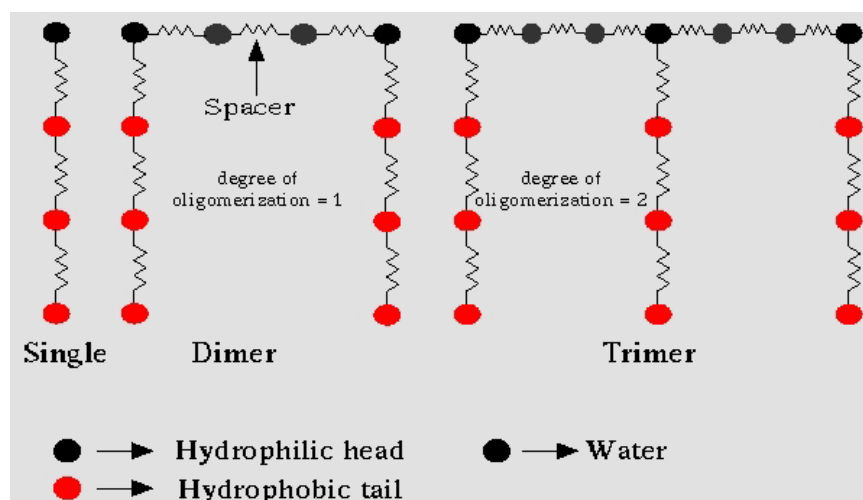
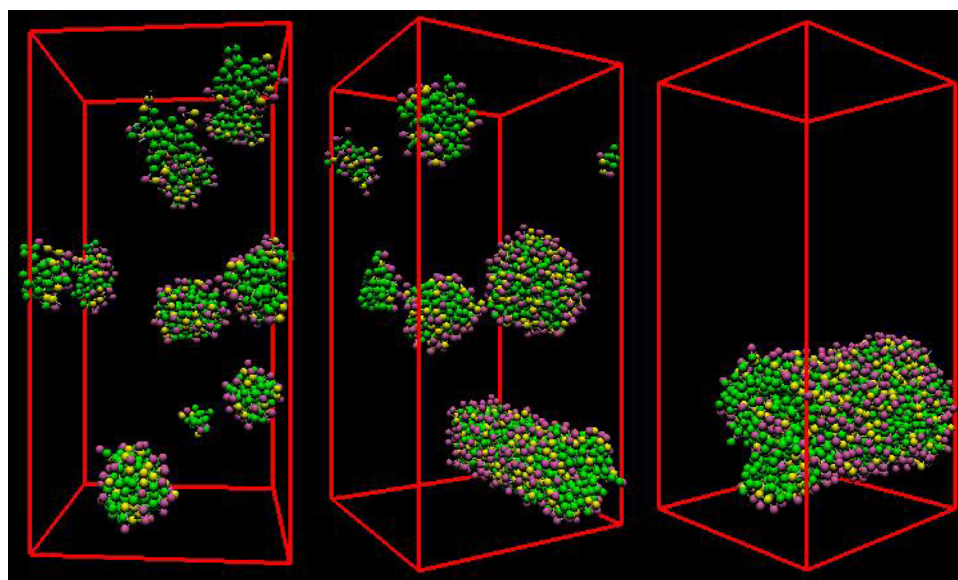


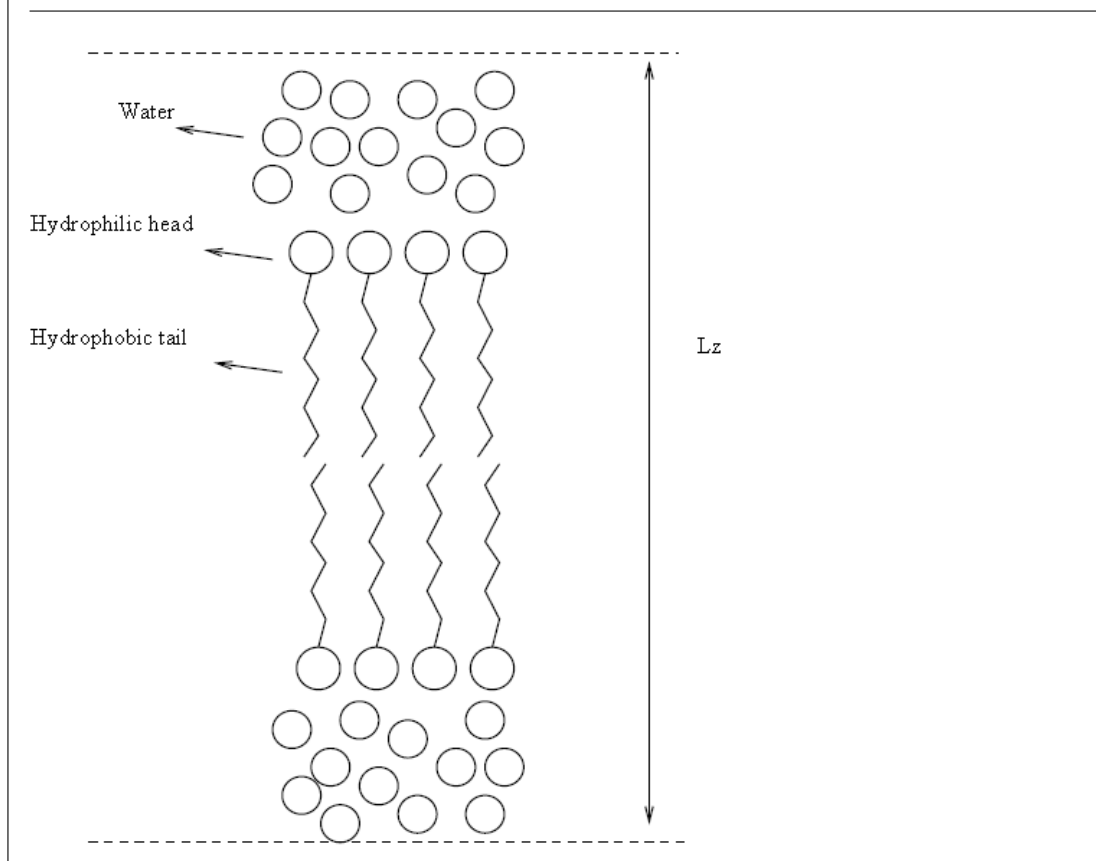
Figure 10: Instantaneous snapshots of the micellar aggregates formed by dimeric surfactants at different concentrations: (a)  $c = 0.004975$ , (b)  $c = 0.0099$ , and (c)  $c = 0.01173$ . The purple, green, and yellow spheres represent the monomers belonging to head, tail, and spacer, respectively. For clarity, water monomers have not been shown in the pictures. Reprinted with permission from [26]. Copyright 2002 American Chemical Society.



single-chain surfactants whose heads are connected by a “spacer” chain, and hence these “double-headed” surfactants are sometimes also referred to as “dimeric surfactants” (see Figure 9). The spacer in dimeric (gemini) surfactants is usually hydrophobic, but gemini surfactants with hydrophilic spacers have also been synthesized [33]. Trimeric surfactants made of three single-chain surfactants connected at

the level of the headgroups by spacer have also been synthesized and their self-assembly properties have been investigated [28, 34]. For dimeric surfactants, the degree of oligomerization  $x$  is 2, and for trimeric surfactants it is 3. We have developed coarse-grained models of the surfactant oligomers as shown in figure 9. The surfactants are modelled as bead-spring models [26, 35, 36] where the beads are either

Figure 11: Schematic of bilayer depicting the periodic cell of height  $L_z$  in the z-direction. z-direction represents bilayer normal.



hydrophilic or hydrophobic. Hydrophilic interaction between like particles (water-water, hydrophilic-water, and hydrophilic-hydrophilic) is modeled via a Lennard-Jones (LJ) potential: inter and intra-molecular interaction can be modelled by empirical forms and the total potential energy is given as follows:

$$E_{\text{total}} = E_{\text{vdW}} + E_Q + E_{\text{bond}} + E_{\text{angle}} + E_{\text{torsion}} \quad (13)$$

where  $E_{\text{total}}$ ,  $E_{\text{vdW}}$ ,  $E_Q$ ,  $E_{\text{bond}}$ ,  $E_{\text{angle}}$ , and  $E_{\text{torsion}}$  are the total energy, the van der Waals, electrostatic, bond stretching, angle bending, and torsion energy components, respectively.

The van der Waals interaction is given by the 12-6 LJ interaction of the following form

$$E_{\text{vdW}}(R) = D_0 \left\{ \left( \frac{R_0}{R} \right)^{12} - 2 \left( \frac{R_0}{R} \right)^6 \right\} \quad (14)$$

where  $D_0$  is the strength of the interaction and  $R_0$  is the range of interaction. Repulsive hydrophobic-hydrophilic and water-hydrophobic interactions are modelled by truncated and shifted LJ potential

also known as Weeks-Chandler-Anderson or WCA potential.

The intra-molecular interaction is described by the bond stretching potential of the following form

$$E_{\text{bond}}(R) = \frac{1}{2} K_b (R - R_0)^2 \quad (15)$$

Angle bending potential

$$E_{\text{angle}}(\theta) = \frac{1}{2} K_\theta (\cos\theta - \cos\theta_0)^2 \quad (16)$$

Torsion potential

$$E_{\text{torsion}}(\phi) = \sum_n \frac{1}{2} V_n [1 - d_n \cos(n\phi)] \quad (17)$$

where  $K_b$ ,  $K_\theta$  are the force constants associated with the bond stretching and angle bending energy.  $R_0$  and  $\theta_0$  are the equilibrium bond length and angle respectively.  $V_n$  is the barrier for the torsion energy. For the self-assembly of surfactant oligomers we have assumed  $K_\theta = 0$ , i.e. the chains are completely flexible. Torsion interactions are ignored as they



Figure 12: (a) Atomistic structure of DPPC and (b) Coarse-grained model of DPPC molecule.

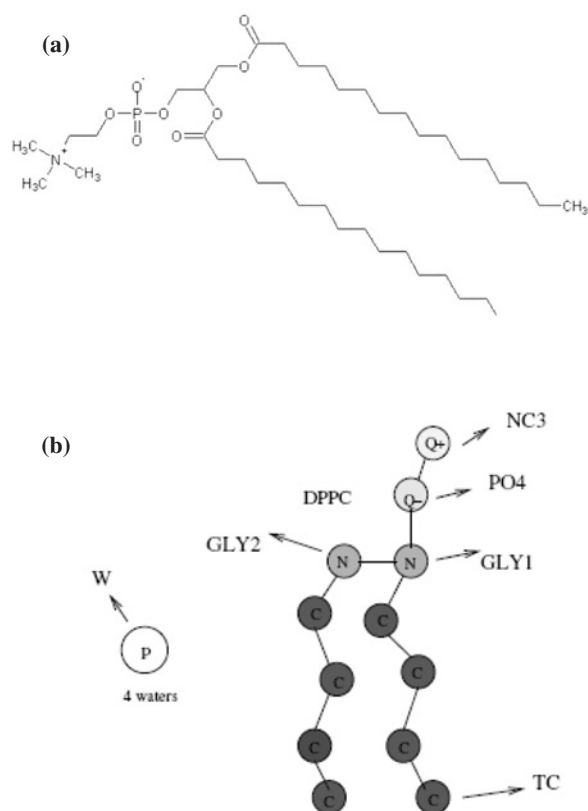
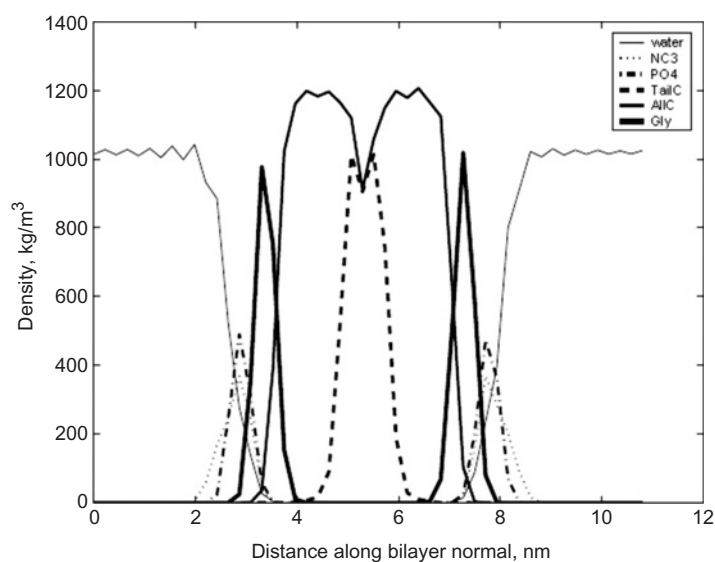
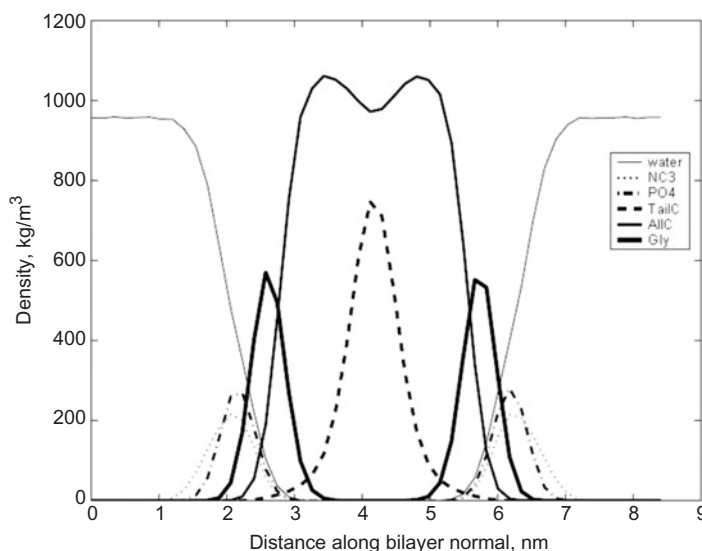
Figure 13: Density distributions along the normal to the bilayer at  $T = 283$  K. The various groups are labelled in Figure 12.

Figure 14: Density distributions along the normal to the bilayer at  $T = 350$  K. The various groups are labelled in Figure 12.



have indirectly included through the non-bond exclusion. Water and oil are modelled as single hydrophilic and hydrophobic beads respectively.

Model surfactant oligomers are initially dispersed at random in a *simulation box* which contains only water and surfactants. Periodic boundary conditions are applied in all the three directions to mimic a bulk system. The surfactant concentration can be expressed either as a mole fraction or in weight fraction. The simulations are performed under constant pressure-constant temperature conditions (NPT) using the Berendsen

weak coupling method [37]. The simulations were carried out for  $P^* = 1$  and  $T^* = 1$  (in reduced units). The number of monomers varies between 25000 and 30000 for different systems. Surfactant mole fraction is defined as  $c = N_a / (N_w + N_a)$ , and  $\rho = (N_a l_a + N_w) / V$  is the total number density of the whole system.  $N_a$  and  $N_w$  are the number of surfactants and water molecules, respectively, and  $V = L_x L_y L_z$  is the volume of the system. We have carried out simulations for a wide range of surfactant concentrations and studied the morphology of the micellar aggregates

Figure 15: Instantaneous snapshots of the bilayer configurations at the end of a 390 ns long coarse grained simulations at  $T = 283$  K and 345 K. For clarity water is not shown.

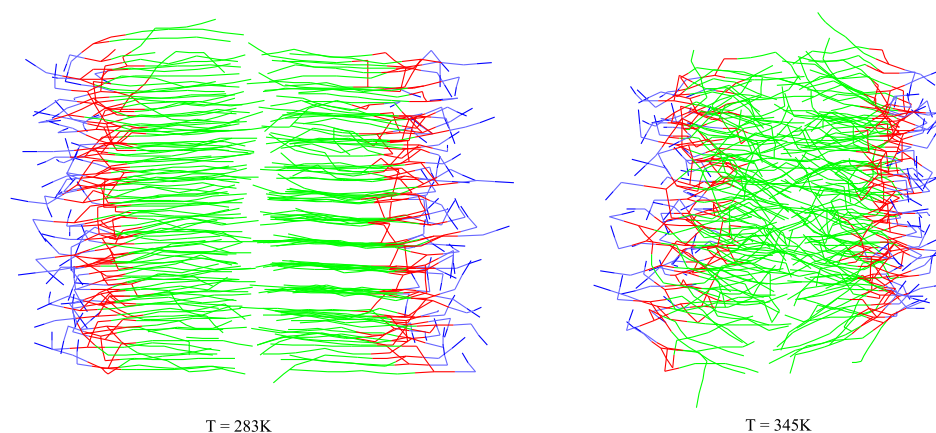


Table 1: Interactions matrix between different coarse-grained beads used in our coarse grained simulations.

Type		P	N				C	Q			
	subtype		o	d	a	da		o	d	a	da
P		I	IV	III	III	II	V	I	I	I	I
N	o	IV	III	III	III	III	III	III	III	III	III
	d	III	III	II	II	II	IV	III	III	II	II
	a	III	III	II	II	II	IV	III	II	III	II
	da	II	III	II	II	I	IV	III	II	II	I
C		IV	III	IV	IV	V	III	V	V	V	V
Q	o	I	III	III	III	III	V	III	III	III	II
	d	I	III	III	II	II	V	III	III	II	I
	a	I	III	II	III	II	V	III	II	III	I
	da	I	III	II	II	I	V	II	I	I	I

formed. For single tail surfactants beyond a critical micellar concentrations we see the formation of micellar aggregates. For the whole range of concentrations simulated we only see the formation of spherical micellar aggregates. In Figure 9 we show the snapshots of micellar aggregates formed by single tail surfactants at various concentrations. To calculate the critical micellar concentration (CMC) we plot the free surfactant mole fraction (surfactant which is not in micellar aggregates) as a function of the surfactant mole fraction and fit it to a line of unit slope which represents the result for a solution of pure monomer. The CMC determination is based on a change in slope of the free surfactant mole fraction curve [38]. In the absence of micelle formation, the free surfactant mole fraction lies on this line and the point where this deviates from linearity indicates the onset of micelle formation and can be considered to be the CMC of the surfactant system. We find that CMC decreases as a function of chain length for single tail surfactants. For surfactant oligomers the CMC decreases as a function of the degree of oligomerization. Figure 10 shows the equilibrium configuration of the micellar aggregates formed by the Gemini surfactants with hydrophobic spacers. We see that with increasing surfactant concentration micellar shape gradually changes from spherical to cylindrical. Our simulation also shows the formation of the worm like and loops like micelles in close agreement with the experimental results.

As a final example of the use of computer simulations in liquid crystals we review the current status in simulating the bilayer phase made of lipids. In this review article we focus on the Dipalmitoyl phosphatidyl choline (DPPC) surfactant solutions and their bilayer phases using coarse grained molecular dynamics simulations. A schematic of a model bilayer along z-direction is shown in Figure 11.

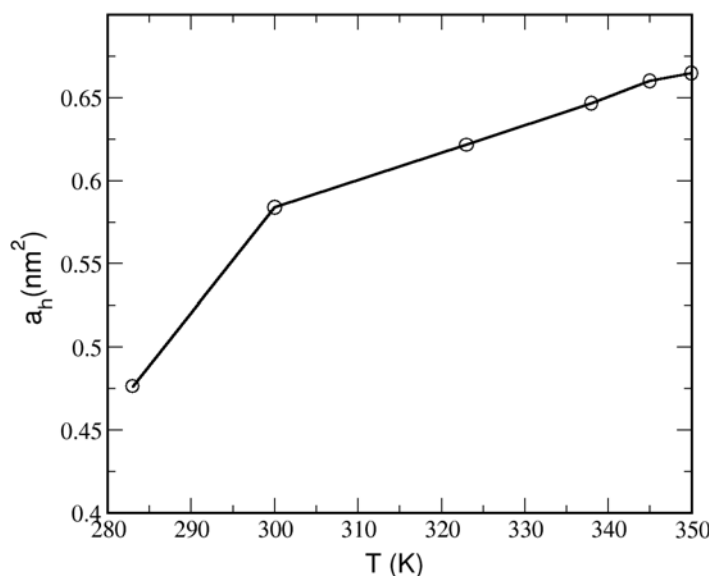
## Coarse-grained simulation of DPPC bilayers

We use the coarse-grained model of DPPC developed by Marrink and co-workers [39, 40]. In this coarse grained model a four to one mapping is used. Four water molecules are represented by a single coarse grained bead. The DPPC molecule is represented by a molecule which has 12 coarse grained beads arranged as shown in figure 12. For computational efficiency identical masses (72 amu) are used for all the beads. The beads are classified into four types: Polar (P), Apolar (C), Non-polar (N), Charged (Q) depending on the nature of the interaction. Polar sites are neutral groups of atoms that would easily dissolve in water. Apolar sites are those which represent hydrophobic sites. Non-polar sites are used for mixed groups which are partly polar and partly apolar. Charged groups represent ionized groups. In the original model, for particle types N and Q there are four sub-types (*o*, *d*, *a*, *da*) depending on nature of hydrogen bonding capabilities. Subtype *o* applies to groups in which no hydrogen bonding capabilities exist. *d* and *a* are for groups that could act as hydrogen bond donor and acceptor respectively. *da* represents groups with both hydrogen bond acceptor and donor options. The non-bonded interactions considered here are LJ and Coulombic interactions. According to the type of particles involved in interaction there are five types of interactions in LJ. These five types have different strengths. For the DPPC case, the zwitterionic PC head group is modeled by a positively charged particle representing choline (NC3) and a negatively charged particle representing the phosphate group (PO4). The glycerol ester linkage is modelled by two non polar particles (GLY1 and GLY2). The two tails are represented by eight apolar particles (C).

There are five levels of interaction in the original model and corresponding strengths are as follows: For level-I (attractive) interaction the strength  $\epsilon$  is 5 kJ/mol, for level-II (semi-attractive) interaction the value is 4.2 kJ/mol, for level-III (intermediate) the value is 3.4 kJ/mol, for level-IV (semi-repulsive) it is 2.6 kJ/mol and for level-V (repulsive) it is 1.8 kJ/mol. The interaction levels between different beads are given in Table 1. The van der Waals radii,  $\sigma_{ij}$ , are similar in all cases and set to 0.47 nm. In the simulations, the LJ potential is cut-off at a distance of  $r_{cut} = 1.2$  nm. To reduce the errors due to truncation, the LJ potential is smoothly shifted to zero between a distance of  $r_{shift} = 0.9$  nm and  $r_{cut}$  using an appropriate shift function. Charged groups interact through the normal electrostatic Coulombic potential.

For our coarse-grained simulations with DPPC bilayer phases we took the final configurations

Figure 16: Area per head group  $a_h$  as a function of temperature showing the gel to liquid crystalline transition at  $T = 300$  K.



of DPPC bilayer phases from the earlier work of Marrink [39]. The system consists of 128 lipid molecules and 1500 coarse grained water beads (equivalent to 6000 water molecules). NPT simulations were carried out at different temperatures with Berendsen temperature and pressure coupling algorithms. We couple the system independently to 1 bar in the lateral and axial directions to mimic a tensionless state. Systems are allowed to equilibrate for up to 50 ns and the properties are evaluated for a subsequent 350 ns. We have used a time step of 4 fs during the simulation.

### Results and discussion

In Figures 13 and 14 we show the density profiles of various components in a direction normal to the bilayer at temperatures 283 K and 350 K respectively. The density distributions are obtained by averaging in the direction parallel to the bilayer by dividing the box in the z-direction. At the lower temperature of 283 K (Figure 13) the bilayer is in the gel phase and the density distributions show increased order in the head group (NC3, PO4, GLY1, GLY2) region. From the density distributions we see that the PO4 and NC3 which represent phosphatidyl and choline groups are within the water. The GLY1 and GLY2 groups which have some affinity to water lie partly in the water region. The bilayer undergoes a phase transition from a high temperature liquid crystalline phase to the gel phase characterized by chain ordering normal to the x-y plane of the bilayer. The instantaneous snapshots of the bilayer at  $T = 283$  K

Table 2: Comparison of area per head group for DPPC at different temperatures with previous simulation and experimental results [39].

T, K	$a_h$ (nm <sup>2</sup> ), this work	$a_h$ (nm <sup>2</sup> ), previous work	experiments $a_h$ (nm <sup>2</sup> )
273	- -		0.46
283	0.4763	0.47 -	
300	0.58387	0.59 -	
323	0.62155	0.64	0.64
338	0.6467	0.66	0.67
345	0.66014	- -	
350	0.6648	- -	

and  $T = 350$  K as shown in Figure 15 illustrate the chain melting. The corresponding area per head group ( $a_h$ ) as a function of temperature is shown in Figure 16. In Table 2 we compare the calculated area per head group with the existing simulation and experimental results on the same system. The results of the simulations are in agreement with those reported in the literature for similar systems [39, 41]. In a periodic system of the bilayer phase, the d-spacing is simply the simulation box dimension in a direction perpendicular to the bilayer plane. Thus  $L_z$  in Figure 11 is the d-spacing. We have also calculated the change in the d-spacing as a function of temperature. A sharp decrease in the d-spacing is observed at the transition temperature of 300 K.

### Conclusion

In this review article we have indicated the manner in which computer simulations can be effectively used to study the phase behaviour of a variety of liquid crystalline systems. The review also illustrates that both molecular dynamics and Monte Carlo simulations can be used with suitable levels of coarse graining to capture the different phases that are observed in experiments. In the first example of banana liquid-crystals the spherocylinder description was able to capture the variety of phases as a function of pressure and the opening angle  $\psi$  using Monte Carlo simulations. In the second example we illustrate the manner in which coarse grained molecular dynamics can be used to study complex microstructure in water-surfactant systems. A simple bead spring coarse grained representation of surfactant oligomers was sufficient to capture the spherical and cylindrical micelles and branched and loop-like micelles observed in these systems. The examples illustrate that with appropriate coarse graining the effects of a fully atomistic description of water and its effects can be adequately captured by a single bead model. Hence this approach opens up the

possibility of investigating mesoscopic structure and dynamics in a computationally efficient manner. Finally the lipid gel to liquid crystalline transition was studied using an atomistically informed coarse grained model for lipid bilayers. This example illustrates that coarse graining can be used to make quantitative predictions which can be compared with experiments.

Received 14 April 2009.

## References

1. D. F. Evans, H. Wennerström, *The Colloidal Domain: Where Physics, Chemistry, Biology, and Technology Meet* (Wiley-VCH, Weinheim Germany, 1999), pp. 672.
2. P. G. de Gennes, J. Prost, *The Physics of Liquid Crystals* (Oxford University Press, New York, 1995), pp. 616.
3. S. Chandrasekhar, *Liquid Crystals* (Cambridge University Press, New York, 2008), pp. 480.
4. M. P. Taylor, J. Herzfeld, *Journal of Physics-Condensed Matter* **5**, 2651 (Apr, 1993).
5. J. Lydon, *Current Opinion in Colloid & Interface Science* **8**, 480 (Apr, 2004).
6. M. R. Wilson, *Chemical Society Reviews* **36**, 1881 (2007).
7. M. R. Wilson, *International Reviews in Physical Chemistry* **24**, 421 (Dec, 2005).
8. S. C. McGrother, D. C. Williamson, G. Jackson, *J. Chem. Phys.* **104**, 6755 (1996).
9. P. Bolhuis, D. Frenkel, *J. Chem. Phys.* **106**, 666 (1997).
10. D. C. Williamson, G. Jackson, *J. Chem. Phys.* **108**, 10294 (1998).
11. J. G. Gay, B. J. Berne, *J. Chem. Phys.* **74**, 3316 (1981).
12. M. A. Bates, G. R. Luckhurst, *J. Chem. Phys.* **110**, 7087 (1999).
13. F. Affouard, M. Kroeger, S. Hess, *Phys. Rev. E* **54**, 5178 (1996).
14. M. R. Wilson, M. P. Allen, *Mol. Cryst. Liq. Cryst.* **198**, 465 (1991).
15. M. A. Glaser, R. Malzbender, N. A. Clark, D. M. Walba, *J. Phys.: Condens. Matter* **6**, A261 (1994).
16. M. Praprotnik, L. Delle Site, K. Kremer, *Annual Review of Physical Chemistry* **59**, 545 (2008).
17. T. Murtola, A. Bunker, I. Vattulainen, M. Deserno, M. Karttunen, *Physical Chemistry Chemical Physics* **11**, 1869 (2009).
18. F. Müller-Plathe, *Chemphyschem* **3**, 754 (Sep, 2002).
19. C. M. Care, D. J. Cleaver, *Reports on Progress in Physics* **68**, 2665 (Nov, 2005).
20. J. C. Shelley, M. Y. Shelley, *Current Opinion in Colloid & Interface Science* **5**, 101 (Mar, 2000).
21. L. Onsager, *Annals of the New York Academy of Sciences* **51**, 627 (1949).
22. M. P. Allen, G. T. Evans, D. Frenkel, B. M. Mulder, *Advances in Chemical Physics* **86**, 1 (1993).
23. T. Niori, T. Sekine, J. Watanabe, T. Furukawa, H. Takezoe, *Journal of Materials Chemistry* **6**, 1231 (Jul, 1996).
24. D. R. Link *et al.*, *Science* **278**, 1924 (Dec, 1997).
25. Y. Lansac, P. K. Maiti, N. A. Clark, M. A. Glaser, *Physical Review E* **67** (Jan, 2003).
26. P. K. Maiti, Y. Lansac, M. A. Glaser, N. A. Clark, Y. Rouault, *Langmuir* **18**, 1908 (Mar, 2002).
27. R. Zana, *Current Opinion in Colloid & Interface Science* **1**, 566 (Oct, 1996).
28. R. Zana, H. Levy, D. Papoutsis, G. Beinert, *Langmuir* **11**, 3694 (Oct, 1995).
29. R. Zana, Y. Talmon, *Nature* **362**, 228 (Mar, 1993).
30. S. Karaborni *et al.*, *Science* **266**, 254 (Oct, 1994).
31. F. M. Menger, C. A. Littau, *Journal of the American Chemical Society* **113**, 1451 (Feb, 1991).
32. F. M. Menger, J. S. Keiper, *Angewandte Chemie-International Edition* **39**, 1907 (2000).
33. L. D. Song, M. J. Rosen, *Langmuir* **12**, 1149 (Mar, 1996).
34. K. Esumi, K. Taguma, Y. Koide, *Langmuir* **12**, 4039 (Aug, 1996).
35. G. S. Grest, K. Kremer, *Physical Review A* **33**, 3628 (May, 1986).
36. M. M. T. Dagama, K. E. Gubbins, *Molecular Physics* **59**, 227 (Oct, 1986).
37. H. J. C. Berendsen, J. P. M. Postma, A. van Gunsteren, A. DiNola, H. R. Haak, *J. Chem. Phys.* **81**, 3684 (1984).
38. D. R. Rector, F. Van Swol, J. R. Henderson, *Molecular Physics* **82**, 1009 (Aug, 1994).
39. Siewart J. Marrink, Alex H. de Vries, A. E. Mark., *J. Phys. Chem. B*, **108**, 750–760 (2004).
40. S. J. Marrink, H. J. Risselada, S. Yefimov, D. P. Tieleman, A. H. de Vries, *Journal of Physical Chemistry B* **111**, 7812 (Jul, 2007).
41. O. Berger., O. Edholm., F. Jahnig., *Biophysical Journal* **72**, 2002–2013 (1997).



**Prabal K Maiti** is Assistant Professor in the Department of Physics, Indian Institute of Science, Bangalore. He works in the area of Multiscale Modeling of Soft and Bio-materials. His major research goal is to pursue theoretical and numerical modeling connecting molecular and macroscopic length scales to improve basic understanding of various soft-matter and biological systems, both from a fundamental and an applied point of view. Areas of current research interest include structure and dynamics of dendrimer, DNA based nanotechnology, DNA-dendrimer complexation and properties of water under strong confinement. Prof Maiti received his M.Sc (1991) and PhD (1998) degree from IIT, Kanpur



**Arun Kumar V** completed his Masters in 2007 from Department of Chemical Engineering, Indian Institute of Science (IISc) under the guidance of Prof. K. G. Ayappa. His area of research includes the study of complex fluids using atomistic and coarse grained molecular dynamics. He has completed his B.Tech in Chemical Engineering from RVR&JC College of Engineering, Nagarjuna University, Guntur in 2005. Currently He is working at Center for Study of Science, Technology and Policy (CSTEP), Bangalore.



**K. G. Ayappa** is Professor in the Department of Chemical Engineering Indian Institute of Science, Bangalore. His research interests lie in probing the structure and dynamics of fluids confined in nanoporous materials, complex fluid interfaces, self assembled structures and phase transitions using statistical mechanics and molecular simulation techniques. Prof Ayappa received his BE degree from Mangalore University in 1984, MS (1987) and PhD (1992) from the University of Minnesota.